AGU PUBLICATIONS

JGR

Journal of Geophysical Research: Atmospheres

RESEARCH ARTICLE
10.1002/2013JD020707

Key Points:
- AgI cloud seeding impact on overshooting deep convection is simulated
- Cloud seeding could potentially modify stratospheric water vapor content
- Increase or decrease in LS water vapor depends on seeding agent amounts

Correspondence to:
B. Chen,
bjchen@nju.edu.cn

Citation:
Chen, B., and Y. Yin (2014), Can we modify stratospheric water vapor by deliberate cloud seeding?, *J. Geophys. Res. Atmos.*, *119*, 1406–1418, doi:10.1002/2013JD020707.

Received 8 AUG 2013
Accepted 8 JAN 2014
Accepted article online 13 JAN 2014
Published online 3 FEB 2014

Can we modify stratospheric water vapor by deliberate cloud seeding?

Baojun Chen[1] and Yan Yin[2,3]

[1]Key Laboratory of Mesoscale Severe Weather/MOE, and School of Atmospheric Sciences, Nanjing University, Nanjing, China, [2]Key Laboratory for Aerosol-Cloud-Precipitation of China Meteorological Administration, Nanjing University of Information Science and Technology, Nanjing, China, [3]Collaborative Innovation Center on Forecast and Evaluation of Meteorological Disasters, Nanjing University of Information Science and Technology, Nanjing, China

Abstract Stratospheric water vapor has an important effect on Earth's climate. Considering the significance of overshooting deep convection in modulating the water vapor content (WVC) of the lower stratosphere (LS), we use a three-dimensional convective cloud model to simulate the effects of various silver iodide (AgI) seeding scenarios on tropical overshooting deep convection that occurred on 30 November 2005 in Darwin, Australia. The primary motivation for this study is to investigate whether the WVC in the LS can be artificially modified by deliberate cloud seeding. It is found that AgI seeding done at the early stages of clouds produces significant effects on cloud microphysical and dynamical properties, and that further affects the WVC in the LS, while seeding at the mature stages of clouds has only a slight impact. The response of stratospheric water vapor to changes in the amount of seeding agent is nonlinear. The seeding with a small (large) amount of AgI increases (decreases) the WVC in the LS, due to enhanced (reduced) production and vertical transport of cloud ice from the troposphere and subsequent sublimation in the stratosphere. The results show that stratospheric water vapor can be artificially altered by deliberate cloud seeding with proper amount of seeding agent. This study also shows an important role of graupel in regulating cloud microphysics and dynamics and in modifying the WVC in the LS.

1. Introduction

Stratospheric water vapor has an important effect on Earth's climate, and the changes in its concentrations can have a significant impact on the trend of global warming [e.g., *Solomon et al*., 2010; *Dessler et al*., 2013]. The water vapor content of the stratosphere is controlled mainly by transport through the tropopause and the oxidation of stratospheric methane [*Ravishankara*, 2012]. The overshooting deep convection as an important mechanism for cross-tropopause transport has attracted researchers' considerable attentions, and significant efforts have been put into both measurements [e.g., *Corti et al*., 2008; *de Reus et al*., 2009; *Iwasaki et al*., 2012] and numerical simulations [e.g., *Wang*, 2003; *Grosvenor et al*., 2007; *Chemel et al*., 2009; *Liu et al*., 2010] to investigate the effects of overshooting convection on the stratospheric water vapor.

Overshooting deep convection can potentially influence the water vapor content entering the stratosphere by injecting ice particles above the tropopause which later evaporate (condensate) and thereby hydrate (dehydrate) the stratosphere. Since the convective vertical transport is the main mechanism for ice particles entering the stratosphere [*Corti et al*., 2008; *Wang et al*., 2011; *Chen and Yin*, 2011, hereinafter referred to as CY11], the amount of ice particles injected into the stratosphere is associated with the ice particle number concentration in the troposphere as well as the strength of convective storms. This has been verified recently by modeling studies of *Liu et al*. [2010] and *Grosvenor* [2010] who found that strong overshoots transported more ice mass and water vapor to the stratosphere relative to weak ones. Accordingly, the physical mechanisms that can stimulate changes in the number concentration of ice particles and the updraft strength for overshooting deep convection have a potential influence on stratospheric water vapor content.

Cloud macrophysical and microphysical properties and precipitation processes of deep convective clouds are affected by atmospheric aerosols which may act as cloud condensation nuclei (CCN) or ice nuclei (IN). This modification of clouds and precipitation by environmental aerosols is also referred to as the inadvertent aerosol seeding of clouds [*Levin and Cotton*, 2009]. A substantial review of aerosol impacts on convective clouds and precipitation has recently been given by *Tao et al*. [2012]. It is shown that CCN or IN may enhance or reduce the updraft strength and precipitation amount depending on the aerosol concentration, as well as

environmental atmospheric conditions [e.g., *Connolly et al*., 2006; *Ekman et al*., 2007; *Li et al*., 2008; *Fan et al*., 2009]. Recently, the CCN effects on overshooting deep convection have also been studied. *Grosvenor et al*. [2007] and CY11 found that the dynamical and microphysical characteristics of tropical overshooting deep convective clouds are affected by changes in CCN concentrations. Their results showed that increases in CCN concentrations can lead to more cloud ice crystals transported to the lower stratosphere (LS), which eventually causes the LS to be moistened as these ice crystals evaporate. And the CCN-induced change in cloud microphysics is found to play a particularly important role in regulating the water vapor content of the LS. Compared to CCN, the effects of IN on stratospheric water vapor have not yet been addressed. Recent modeling studies [e.g., *Fan et al*., 2010; *Zeng et al*., 2013] have shown that IN has a significant impact on the anvil properties (e.g., areas, ice number, and mass) of tropical deep convective clouds and in turn further affects water vapor content in the tropopause region [*Fan et al*., 2010]. However, it is not clear whether IN can affect the water vapor content of the stratosphere.

Silver iodide (AgI) is a special type of IN. Since its effectiveness as a nucleus for ice crystal formation, AgI plays a particularly important role in weather modification. Convective cloud seeding with AgI has been carried out worldwide as a technique for enhancing precipitation or mitigating hail fall over the last several decades [*NRC*, 2003; *Qiu and Cressey*, 2008]. In contrast to the inadvertent cloud seeding by background atmospheric aerosols, the artificial seeding with AgI is a deliberate modification of clouds and precipitation by additionally injecting appropriate amount of AgI particles into a supercooled cloud in specific time and location, for the purpose of enhancing the formation of ice crystals and stimulating precipitation by ice particle growth so that the cloud seeding can be artificially controlled. Previous studies have suggested that AgI seeding had a large effect on the microphysical and dynamical properties of convective clouds and found that cloud microphysical changes induced by seeding played a very important role in determining storm development and precipitation [e.g., *Orville and Chen*, 1982; *Rosenfeld and Woodley*, 1993; *Farley et al*., 2004; *Ćurić et al*., 2007, 2008; *Chen and Xiao*, 2010; *Xue et al*., 2013]. Modeling results of *Farley et al*. [2004] and *Chen and Xiao* [2010] also showed an evident increase in the ice content in the upper tropospheric regions of convective clouds due to seeding. This suggests that there is a possible link between AgI seeding of deep convective clouds and stratospheric water vapor.

This paper extends the work of CY11 to explore the impact of AgI seeding on tropical deep convective clouds. The fundamental difference is that in the CY11 study, the inadvertent effects of background aerosols were examined, whereas here the primary goal is to investigate whether the water vapor content in the LS can be artificially modified by deliberate cloud seeding. We address this issue by performing a series of sensitivity experiments using the same cloud model and storm case in CY11. The next section briefly describes the model and experimental design. Results from the sensitivity experiments are discussed in sections 3 and 4. Finally, the summary and conclusions are presented in section 5.

2. Model and Experimental Design

2.1. Model Description

The model being used in this study is a three-dimensional, nonhydrostatic, and fully compressible convective cloud model, developed by *Kong et al*. [1990] based on the dynamic framework of *Klemp and Wilhelmson* [1978]. The original microphysics parameterization adopted in the model is a one-moment bulk scheme that predicts only the mixing ratio of the hydrometeor species. A two-moment bulk scheme with AgI seeding processes developed by *Hong and Fan* [1999] is subsequently implemented into the model to study hail formation mechanisms and seeding effects in hailstorms. The explicit droplet nucleation (CCN activation) was recently included in the model by CY11 based on *Rogers and Yau* [1989] and *Morrison et al*. [2005] to investigate CCN impacts on overshooting convection and stratospheric water vapor. The modified version of CY11 was used in the present study to perform the simulation. In the current version, the model predicts the evolution of mass mixing ratios as well as the number densities of the seven hydrometeor types cloud droplets, raindrops, cloud ice, snow, graupel, frozen drops, and hail. The mixing ratio of AgI seeding agent is also predicted explicitly. For a detailed description of model dynamics and microphysics, please refer to *Hong and Fan* [1999], or *Chen and Xiao* [2010] and *Chen and Yin* [2011]. Only the key processes pertinent to this work are described here.

Ice crystals are formed by three microphysical processes: primary nucleation due to deposition and condensation freezing occurring on active natural ice nuclei, secondary ice production or ice multiplication, and

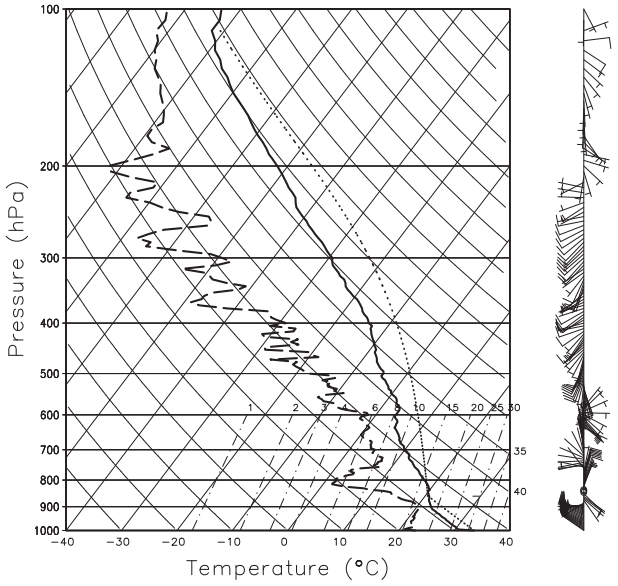

Figure 1. Skew-*T* log-*p* diagram plotted from the sounding taken in Darwin at 1430 local time, 30 November 2005. Wind vectors are shown on the right border (a full barb = 10 kt and a half barb = 5 kt). Adapted from *Chen and Yin* [2011].

homogeneous freezing of cloud droplets. For primary ice nucleation, the number of ice crystals initiated from natural ice nuclei is specified as a function of temperature according to *Cooper* [1986] and given by:

$$N_i = 0.005 \exp\left[0.304(T_0 - T)\right], \quad (1)$$

where $T_0 = 273.15$ K, T is the ambient air temperature (K), and N_i is the number of ice crystals initiated (L^{-1}). For the current study, cloud ice is allowed to initiate by equation 1 only when the water vapor mixing ratio exceeds 25% supersaturation with respect to ice or water saturated and $T < 260$ K, following *Thompson et al.* [2008]. Ice multiplication is specified to be the Hallett-Mossop riming/splintering mechanism occurring at temperatures between −3°C and −8°C and is parameterized following *Hu and He* [1988]. Homogeneous freezing of cloud droplets is assumed to occur instantaneously at temperatures lower than −40°C. Once cloud ice forms, it grows by vapor deposition and riming processes. If cloud ice falls into warm ($T > 0$°C) air, it melts instantly to cloud water.

Snow is formed by depositional growth and riming of ice crystals and also by the collision and aggregation of ice crystals. Snow continues to grow by deposition or collection of cloud ice and cloud water. Cloud ice and snow can be converted to graupel by riming. The autoconversion rate coefficient for cloud ice to snow and snow to graupel is based on *Lin et al.* [1983]. Graupel may be also generated by probabilistic freezing of raindrops and collisional freezing of rain with cloud ice, snow, or AgI particles when the raindrop diameter is smaller than 1 mm. The freezing of large raindrops (diameter more than 1 mm) is converted to frozen drops. The density of frozen drops is set to a fixed value of 0.9 g cm^{-3}. While the density of graupel varies with the graupel content and is assumed to be 0.12 g cm^{-3} if the graupel content is less than 0.5 g m^{-3}; otherwise, it is assumed to be 0.4 g cm^{-3}. Once generated, graupel and frozen drops may grow by collection of cloud water, rain, cloud ice, and snow, or by vapor deposition. Graupel and frozen drops are converted to hail when their diameters are greater or equal to 5 mm. It has been shown by *Kovačević and Ćurić* [2013] that the microphysics scheme distinguishing graupel and frozen drops is better for simulation of precipitation in convective clouds.

The scheme employed here to initialize ice formation by AgI is mainly based on *Hsie et al.* [1980]. Following this scheme, the AgI particles are assumed to be monodisperse with a radius of 0.1 μm and a mass of 2.38×10^{-17} kg. The terminal velocity of AgI particles is neglected. The nucleation mechanisms by which AgI can produce ice crystals include condensation-freezing/deposition nucleation and contact freezing nucleation. Contact nucleation mechanisms are limited to inertial impact and Brownian collection. Only one active AgI particle can be captured by one liquid drop for contact freezing nucleation. But impact scavenging of AgI particles by raindrops is not considered here. The graupel and frozen drops can be also formed by contact freezing of raindrops with AgI particles. The relevant seeding parameterizations have been described in detail by *Hong and Fan* [1999] and *Chen and Xiao* [2010], which will not be repeated in this work. The nucleating efficiency of AgI is based on a fitting temperature-dependent activation curve [*Hsie et al.*, 1980]. Activation only occurs in the cloudy environment and when the temperature is below −5°C. If the temperature is further colder than −20°C, all of the AgI particles are activated, and the maximum number concentration of active nuclei is 160 L^{-1} approximately. For the temperature between −5 and −20°C, the number of active nuclei, N_a (L^{-1}), is prescribed as a function of temperature and given by [*Hsie et al.*, 1980]:

$$N_a = \exp\left[-0.022(T_0 - T)^2 + 0.88(T_0 - T) - 3.8\right], \quad (2)$$

where T is the ambient air temperature (K), and $T_0 = 273.15$ K.

Table 1. Some Features for Cases t20z60[a]

Cases	X_{S0} (g g^{-1})	[AgI] (g)	TMASS (KT)	TP (KT)	Ipart (%)	IWM_{LS} (%)	WVM_{LS} (%)	W_{TROP} (m s^{-1})	W_{LS} (m s^{-1})
unseeded	/	/	54,515.0	39,824.4	50.7	/	/	43.1	16.8
1	2.0×10^{-13}	12	54,749.3	40,005.7	51.2	+16.6	+0.092	43.3	16.3
2	1.0×10^{-12}	61	55,186.9	40,552.6	51.8	+26.9	+0.150	43.2	15.5
3	3.0×10^{-12}	184	55,677.5	41,153.5	52.1	+29.8	+0.172	43.0	15.2
4	8.0×10^{-12}	490	56,448.8	41,969.2	52.7	+27.5	+0.148	42.5	15.3
5	1.7×10^{-11}	1042	57,672.5	43,099.7	54.1	+10.9	+0.039	42.0	15.7
6	3.0×10^{-11}	1839	58,500.4	43,967.8	54.8	+8.37	+0.005	41.9	15.6
7	4.5×10^{-11}	2758	59,537.1	45,137.8	55.8	−3.85	−0.053	41.5	15.5
8	8.0×10^{-11}	4904	60,511.3	46,257.1	56.7	−9.52	−0.091	41.3	15.3
9	1.5×10^{-10}	9195	61,650.9	47,605.7	58.0	−14.4	−0.120	41.2	14.8
10	3.0×10^{-10}	18,390	62,462.5	48,639.2	58.9	−16.0	−0.136	41.0	14.1
11	5.0×10^{-10}	30,650	62,882.8	49,026.8	59.5	−8.96	−0.114	40.2	14.3
12	1.0×10^{-9}	61,300	63,297.3	49,344.7	60.4	−7.11	−0.102	40.4	14.4

[a] X_{S0} is maximum value of the initial AgI mixing ratio; [AgI] is total amount of seeding agent injected in the domain; TMASS and TP are accumulated total mass of condensate and precipitating hydrometeors (rain, snow, graupel, frozen drops, and hail), obtained from the integration over the entire domain and duration time, respectively; Ipart is ice-phase hydrometeor (cloud ice, snow, graupel, frozen drops, and hail) mass partitioning in the storms; IWM_{LS} and WVM_{LS} are seeding-induced changes in cloud ice and water vapor mass in the LS expressed in percentage, respectively. Maximum updraft velocity in the storm and LS is represented by W_{TROP} and W_{LS}, respectively.

2.2. Experimental Setup

The overshooting deep convection that developed on 30 November 2005 in Darwin, Australia, during the Stratospheric-Climate Links with Emphasis on the Upper Troposphere and Lower Stratosphere/Aerosol and Chemical Transport in Tropical Convection (SCOUT-O3/ACTIVE) campaign was simulated in the present study. Figure 1 shows the profiles of temperature and dew-point temperature taken from Darwin, on 30 November 2005 at 1430 LT, which presents a very large convective available potential energy of approximately 3500 J kg^{-1}. The wind hodograph shows a weak vertical wind shear and a small horizontal wind speed of less than 5 m s^{-1} in the troposphere. We have examined the impacts of initial CCN concentrations on the simulated storm characteristics and stratospheric water vapor content in CY11. Here the model setups were similar to those of CY11. All of the simulations were integrated to 4200 s using a horizontal grid spacing of 0.5 km over a 41 km × 41 km domain and a vertical grid spacing of 0.3 km over a 24 km depth. For a given spatial resolution, the model uses the large time step of 2 s and the small one of 0.25 s, respectively. Convection was initiated by a warm bubble of 20 km wide and 3 km deep, placed at 1.5 km above ground level and at the horizontal center of the model domain. The maximum thermal perturbation was 2 K in the center of the bubble, with the amplitude decreasing according to a $\cos^2$ relationship with radial distance from the center. Sensitivity tests showed that such heating overall produced a better simulation as compared to the radar observations [refer to CY11]. Considering that the cold point tropopause was situated at 17.3 km altitude for the current event [*de Reus et al*., 2009] and the vertical grid size used in the simulations, the LS boundary herein is defined at 17.4 km.

The initial distribution of the seeding agent, similar to *Hsie et al*. [1980] but extended vertically and horizontally over three grid points, which forms a cubic block, has maximum values in the center and decreases with distance outward. The seeding agents were released continuously for 300 s, and the height of the center of the initial seeding agent is located at 6.0 km level (−5°C approximately). Two groups of seeding experiments have been carried out to investigate the effects of various seeding scenarios. The first one (denoted by t20z60) was seeded in the region of the strongest updraft when the model cloud top was passing the −10°C level at 20 min (cloud-growing stage). The other one (denoted by t30z60) is designed to test the effects of time of the seeding agent released by seeding at a later time, that is, 10 min later than in t20z60 when the simulated storm is at the mature stage. Considering that the number concentrations of ice particles nucleated newly by seeding are closely related to the seeding agent amount, for each seeding group, we design 12 sensitivity runs with the core values of the AgI mixing ratio ranging from 2×10^{-13} g g^{-1} to 1×10^{-9} g g^{-1} to survey the response of the LS water vapor content to the changes in the amount of AgI seeding agent (hereinafter referred to as [AgI]). Specific values used in the present simulations are listed in Table 1. Cloud features of sensitivity experiments from cases t20z60 are also shown in the table as this seeding group obtained a more significant effect relative to the other group. Since the primary motivation for this study is to address the possibility of artificially modifying stratospheric water vapor, the background aerosol impacts on

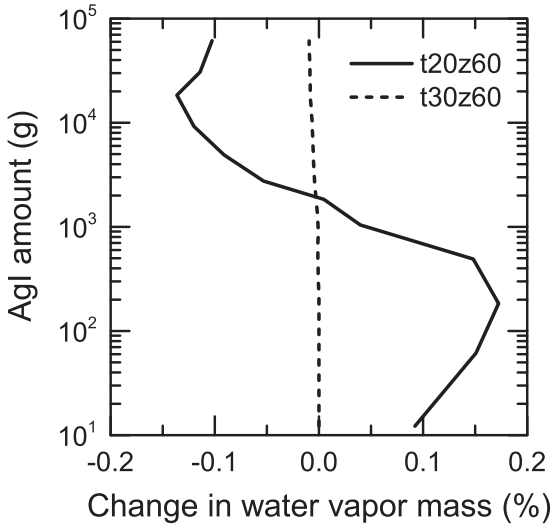

Figure 2. Changes in accumulated total water vapor mass in the lower stratosphere as a function of the total silver iodide (AgI) amount injected into the domain, relative to the unseeded case. Solid and dashed lines represent the t20z60 and t30z60 cases, respectively. A positive value means an excess for the seeded case.

the seeding effects are not considered. All of the numerical experiments are assumed to perform at the maritime CCN scenarios. In other words, the current research focuses on maritime convective storms.

3. Does Seeding Affect LS Water Vapor Content?

Figure 2 shows the seeding-induced percentage change in the accumulated total mass of water vapor in the LS that is the overall amount produced throughout the integration. A positive (negative) value means an excess (a loss) for the seeded case relative to the unseeded case. Comparing the two seeding groups, the change in water vapor mass for cases t30z60 (dashed line) is much smaller, even under the condition of extremely high [AgI] (maximum magnitude only 0.01% approximately). Whereas a large variation is found for cases t20z60 (solid line), ranging from −0.136% to +0.172% (Table 1). The results show that the AgI seeding does not modify the water vapor content of the LS significantly when the seeding was carried out at the mature stage of convective storms. When the seeding was carried out at the early cloud-growing stage, however, the seeding has a large influence on the LS water vapor. With the mean over the stratospheric domain and over the whole 70 min integration, the seeding-induced increase or decrease in water vapor mixing ratio reaches a maximum of 1.463 ppbv and −1.114 ppbv, respectively. Compared with the background water vapor mixing ratio of 1.435 ppmv derived from the initial sounding, the seeding-induced change is 1‰ approximately.

At the end of the simulation, the total mass of water vapor in the LS for seeded cases is increased by ~4.3–5.7% compared to the simulation start. For unseeded case, the water vapor mass is found to be increased by 5% [CY11]. Hence, based on the comparison between the unseeded and seeded cases, it is concluded that seeding leads to an extra moistening of the LS up to ±0.7%.

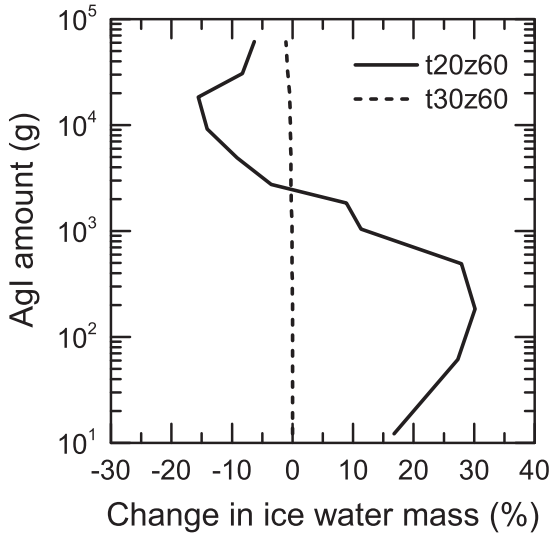

Figure 3. As Figure 2 but for total ice mass.

Given the significance of ice particles of the LS in determining the stratospheric water vapor content [e.g., *Corti et al.*, 2008; *Chemel et al.*, 2009; CY11], it is necessary to examine the seeding effects on stratospheric ice particles. Figure 3 presents the changes induced by seeding in the total mass of ice hydrometeors (cloud ice, snow, graupel, frozen drops, and hail) in the LS. One can see that the LS ice mass is affected significantly for cases t20z60, showing a −15.5% to +30.1% change. Compared to t20z60, the change in ice mass is insignificant for cases t30z60. The results show that seeding at the early stages of storms can modify the stratospheric ice mass significantly.

As shown in Figures 2 and 3, both the ice and water vapor mass in cases t30z60 decrease slightly due to seeding, and the magnitude of reduction increases with increasing [AgI]. From the results of cases t20z60, it is found that both the ice and water vapor mass in the LS change

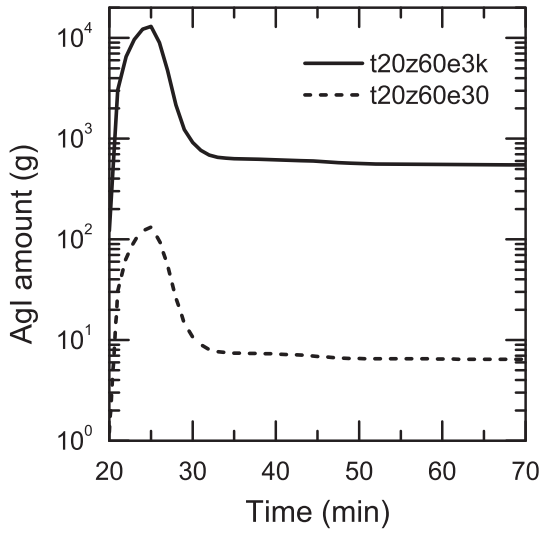

Figure 4. The amount of AgI seeding agent in the model domain as a function of time for cases t20z60e3k (solid line) and t20z60e30 (dashed line).

nonlinearly with [AgI]: increase in the low [AgI] runs but decrease in the high [AgI] runs, indicating that the seeding with a small (large) amount of AgI seeding agent leads to more (less) ice and water vapor in the LS. This critical seeding amount is ~2000 g in this case. The results suggest that the response of the water content in the LS to changes in the seeding agent amount is nonlinear, and this is likely due to the complicated interaction between cloud microphysics and dynamics. Detailed analysis on the seeding effects will be presented in the following sections. Note that the accumulated total ice mass and total water vapor mass in seeded cases shown in Figures 2 and 3 exhibit similar changes; this is because sublimation of injected ice particles from troposphere is an important contributor to stratospheric water vapor [e.g., CY11]. The figures also suggest that the stratospheric water vapor would be potentially increased or decreased further given more time.

4. Mechanisms Affecting LS Water Vapor

4.1. Sinks and Conservation of Seeding Agent

In this section, a representative pair of experiments from the group of t20z60, denoted t20z60e30 and t20z60e3k, which obtained the greatest increase (+0.172%) and decrease (−0.136%) in the LS total water vapor mass, respectively, were selected to analyze the seeding effects. These two cases are run with the same initial conditions except that t20z60e3k is seeded with a larger amount of seeding agent. At the time of initial seeding (at 20 min), the simulated cloud top has already reached the 7.2 km altitude (−13.4°C level), and the updraft core is located at 4.5 km with a maximum value of 23.4 m s^{-1}. With being released in the seeding region continuously, the amount of AgI seeding agent in the domain increased gradually and reached its peak at the end of seeding (at 25 min) for both the two cases (Figure 4). Approximately a total of 184 and 18,390 g of AgI were injected for t20z60e30 and t20z60e3k, respectively. Most of the seeding agent has been nucleated within 5 min after seeding (25–30 min), accounting for over 80% of the total consumption. At the end of simulation, the total consumption of seeding agent is 162 and 16,313 g in t20z60e30 and t20z60e3k, respectively, accounting for over 88% of the seeding amounts. This indicates that only 8% of AgI is decreased due to strong advection through the boundaries, because of less than 4% of seeding agent remaining in the domain by the end of the simulation. Overall, conservation of the seeding agent mass is good. Deposition nucleation or condensation-freezing nucleation is the most important mechanism responsible for cloud ice production by seeding, accounting for 97.5% of the total sink of the seeding agent. Contact freezing of raindrops, mainly through the Brownian motion mechanism, is the second largest AgI sink, with a 2% contribution. Other nucleation modes contribute less than 0.5%.

4.2. Dynamical and Microphysical Effects of Seeding on Storms

The effects of seeding on storm dynamics are first examined. For the current event, the upward transporting ice particles across the tropopause are found to occur during the time period 30–34 min and 38–50 min, which correspond to the strongest stage of the storm life cycle and the local stratospheric convection developing stage, respectively (see CY11). The cross-tropopause transport of ice particles into the LS at the first stage is largely determined by the storm main updraft, while the LS updraft dominates the second stage. The maximum storm main updraft velocity is 43.1 m s^{-1} occurring at 32 min and 13.2 km altitude in the unseeded case. For case t20z60e30, the maximum main updraft velocity is 43.0 m s^{-1}, occurring at 31 min and 12.9 km altitude. One can see that the peak updraft velocity in t20z60e30 is almost the same as in the unseeded case. This suggests that for the light seeding case, seeding does not induce much dynamic change. For case t20z60e3k, the maximum updraft velocity is 41.0 m s^{-1}, occurring at 31 min and 12.6 km altitude.

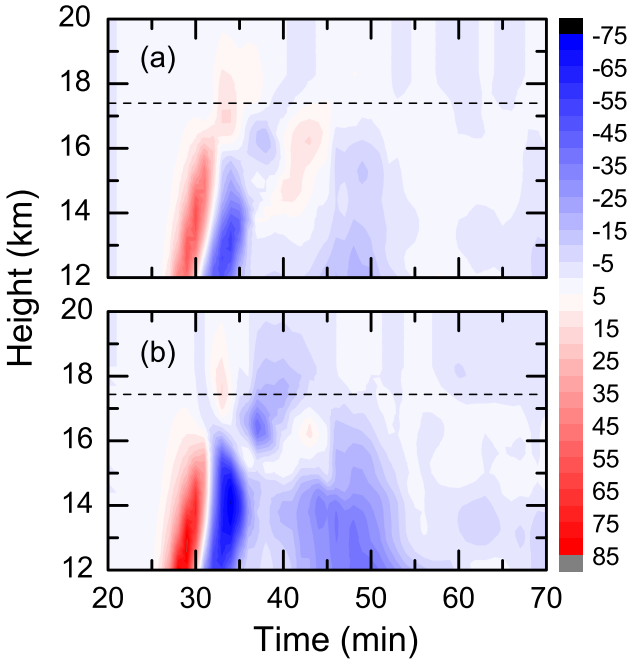

Figure 5. Time vs height section of the differences between the seeded (t20z60e30 in Figure 5a, and t20z60e3k in Figure 5b) and unseeded cases in areally integrated updraft mass flux (10^6 kg s^{-1}). Dashed line indicates the 17.4 km altitude, here defined as the lower boundary of the stratosphere.

Compared to the unseeded case, case t20z60e3k has a weaker updraft and a lower updraft core. Seeding also affects updraft intensity in the stratosphere. It is found that a weaker cold trap region near the tropopause is formed in the seeded case, thus resulting in a weaker descent above the cloud top and a weaker convection in the LS, with the maximum updraft of 15.2 m s^{-1} for t20z60e30 and 14.1 m s^{-1} for t20z60e3k, respectively, as compared to the unseeded case, which has a stratospheric updraft maxima of 16.8 m s^{-1}. These results indicate that AgI seeding weakens the intensity of tropical overshooting convection.

Changes in updraft velocities can further affect the upward transport of air mass. Figure 5 shows the change in updraft mass flux due to seeding at a given time and altitude, which is computed from, and ρ_a is air density, w is updraft magnitude, and A is area. One can see that tropospheric updraft mass flux in both seeded cases is increased before 30 min, i.e., within 5 min after seeding, and is decreased thereafter. The increase or decrease in case t20z60e3k is even larger. Significant changes in updraft mass flux crossing the tropopause can be found to occur after 30 min when the simulated storm evolves into the mature stage. Roughly, the early flux is increased, and the later is decreased in both cases. The net flux is still increased in t20z60e30 and is decreased in t20z60e3k, suggesting that there would be more (less) transporting upward into the LS in t20z60e30 (t20z60e3k).

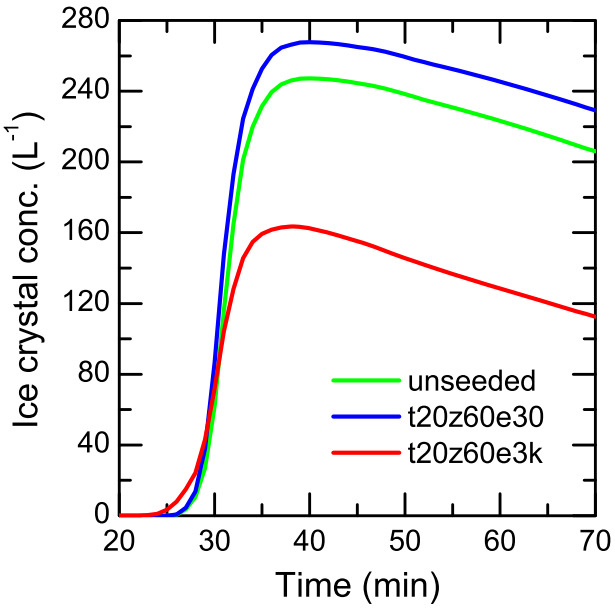

Figure 6. Comparison of the temporal evolution of domain-averaged number concentration of the ice crystals in the troposphere (below 17.4 km in this work) for the unseeded (green) and two seeded cases: t20z60e30 (blue) and t20z60e3k (red).

During the upward transporting ice particles across the tropopause, the number of ice crystals in the troposphere is key to determining the ice mass in the LS. In our simulations, ice crystals dominate the LS accounting for ~99.98% of the total hydrometeor number concentration. By comparison, the other ice hydrometeors (snow, graupel, frozen drops, and hail) contribute less than 0.02% of the total, and hence their contributions to the change in stratospheric water vapor content are negligible when compared to the ice crystals. Figure 6 shows the temporal evolution of domain-averaged number concentration of ice crystals in the troposphere for the unseeded and two seeded cases. The tropospheric region herein is defined below 17.4 km referred to the tropopause height and the vertical grid size used in the simulations. One can see that the difference in

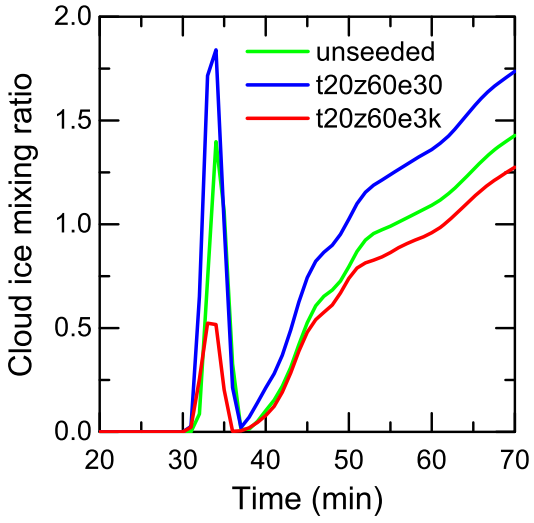

Figure 7. Time evolution of the domain-averaged cloud ice mixing ratio (10^{-3} g kg^{-1}) in the lower stratosphere for the unseeded (green) and two seeded cases: t20z60e30 (blue) and t20z60e3k (red).

ice crystal concentrations between seeded and unseeded cases is small in the early seeding stage. After 30 min, however, the ice crystal concentration evolution shows a large difference in the two seeded cases. Case t20z60e30 has more ice crystals in the troposphere than the unseeded case; in contrast, the ice crystal concentration is significantly lower in t20z60e3k than that in the unseeded case. Overall, the ice crystal concentration has been increased by 9.6% in t20z60e30 but decreased by −37.6% in t20z60e3k, showing that more (fewer) ice crystals are produced in light (heavy) seeding case.

Previous study by CY11 has shown that ice crystals in the stratosphere are transported upward by overshooting convection from the troposphere. The overshooting activity in the simulated case begins at 30 min. Figure 7 shows the time evolution of the cloud ice mixing ratio averaged over the LS domain for seeded and unseeded cases. One can see that cloud ice occurs in the LS after 30 min, and the content exhibits a similar trend for the three cases. Compared to the unseeded case, during the period covering the overshooting, more (less) cloud ice entered the stratosphere due to enhanced (reduced) vertical transport and increased (decreased) tropospheric ice crystal concentrations for t20z60e30 (t20z60e3k).

How does seeding affect cloud ice production? The differences between the seeded and unseeded cases for various production terms for cloud ice concentrations versus time are shown in Figure 8. Differences in rime splintering multiplication are insignificant and are not included. Comparing Figures 6 and 8, the initial increase in cloud ice concentrations in t20z60e3k is clearly due to the seeding by which water vapor is converted to cloud ice (NUxai). The later decrease in cloud ice concentrations is due to the decrease in homogeneous freezing of droplets (HFZci) and deposition nucleation on natural ice nuclei (NUvi). In the model, natural deposition nucleation is based on a temperature-dependent scheme given in equation 1. Nevertheless, changes in water vapor content may have an impact on deposition nucleation because it is limited to occur only when the air is saturated with respect to water and $T < 260$ K or the water vapor mixing ratio exceeds 25% supersaturation with respect to ice. Seeding decreases the water vapor content, thereby resulting in the reduction in cloud ice production through natural deposition nucleation. Compared with the difference between t20z60e3k and unseeded case in NUxai and NUvi, the seeding-induced change in the two production terms is very small for case t20z60e30 (solid lines in Figure 8).

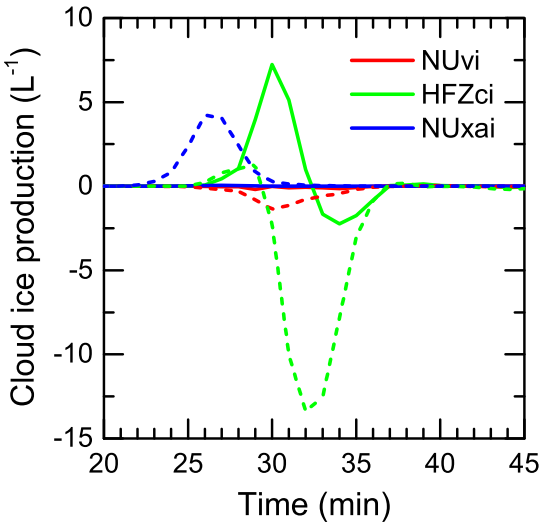

Figure 8. The differences in the production terms for cloud ice concentrations as a function of time between the seeded and unseeded cases. Solid and dashed lines represent the case t20z60e30 and t20z60e3k, respectively. NUvi and NUxai denote the primary nucleation of cloud ice occurring on natural ice nuclei and AgI particles, respectively. HFZci is homogeneous freezing of cloud droplets. A positive value means an excess for the seeded case.

The seeding influences homogeneous freezing of droplets to form ice crystals significantly. In our simulations, the main sinks for cloud water are accretion by rain, graupel, frozen drops, and hail and homogeneous freezing. Collection of rain is the largest sink for cloud water and dominates the cloud water content. Seeding reduces the collection of cloud water by rain during 20–30 min because of the enhanced depletion of the rain water through the accretion by the early seeding-

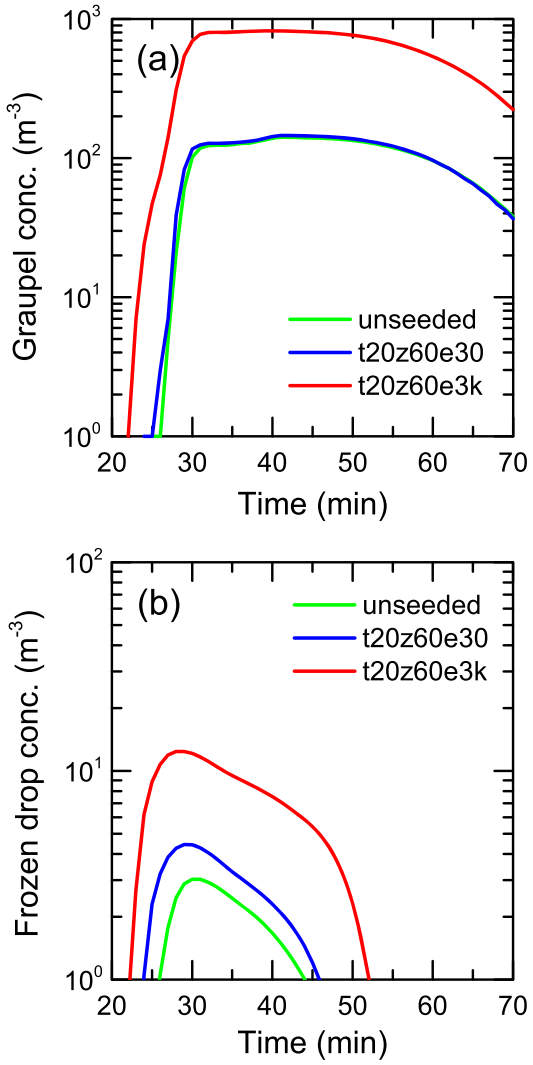

Figure 9. Domain-averaged number concentration of (a) graupel and (b) frozen drops in the troposphere for the unseeded case (green) and the seeded cases of t20z60e30 (blue) and t20z60e3k (red).

increased ice crystals and AgI particles. Despite the earlier formation and increased amounts of graupel and frozen drops in seeded cases (Figure 9) enhance the depletion of the cloud water due to the riming process at the same time, the cloud water is still greater in the seeded case than in the unseeded case, because the decreased depletion of the cloud water by the rain collection is much greater than the increased depletion by the riming process on graupel or frozen drops. With the enhanced transporting upward at earlier times in seeded cases (Figure 5), more cloud water can ascend to altitudes where the homogeneous freezing is initiated (the fall velocity of droplet is neglected in this study), resulting in the increase in homogeneous freezing of cloud droplets. Note that this increase is more significant in t20z60e30 than that in t20z60e3k. This is because the seeding increases only slightly the concentration of graupel and frozen drops for t20z60e30 and thus depletes less cloud water compared with t20z60e3k. As simulated storms evolve into the mature stage, the riming of graupel and frozen drops is the most important depletion terms of supercooled cloud water. As is indicated in Figure 9, the seeding causes substantial increases in graupel and frozen drops after 30 min for t20z60e3k, as a result, less cloud water available for the homogeneous freezing which is decreased significantly in the seeded case. Compared with t20z60e3k, the decrease in the homogeneous freezing is small for t20z60e30, since the seeding has only slightly increased the concentration of graupel and frozen drops. Overall, for t20z60e30 (t20z60e3k), the increased amounts of ice crystals at the earlier time through the homogeneous freezing of cloud droplets are markedly greater (smaller) than the decreased amount at the later time, thus leading to more (less) cloud ice produced in the seeded case as compared to the unseeded case.

Both graupel and frozen drops are increased by seeding (Figures 9a and 9b). Nevertheless, frozen drops are found to play a small role in seeding effects because their concentrations are substantially low. On average, the number concentration of frozen drops is two orders of magnitude lower than that of graupel approximately. This is due to the fact that frozen drops are generated only by the freezing of large raindrops, while graupel can be formed by the freezing of small raindrops, or by aggregation of ice crystals or snow. Note that the differences between t20z60e3k and unseeded case for graupel concentrations are much pronounced, showing a 505% increase in the total compared to the unseeded case. In contrast, t20z60e30 does not produce significant differences compared to t20z60e3k (the total concentration of graupel increases only 3.4%). The main mechanisms by which seeding causes increases in graupel production are the collisional freezing of raindrops with AgI and seeding-increased ice crystals or snowflakes. Their production rates are directly related to the number of AgI particles and increase with increasing seeding agent amounts. The insignificant differences between t20z60e30 and unseeded case are due to the reason that the amount of AgI used in the experiment is much less.

The seeding results in substantial increases in graupel particles for t20z60e3k. These large amounts of graupel particles grow by riming and deposition enhancing depletion of droplets and water vapor, leading to the

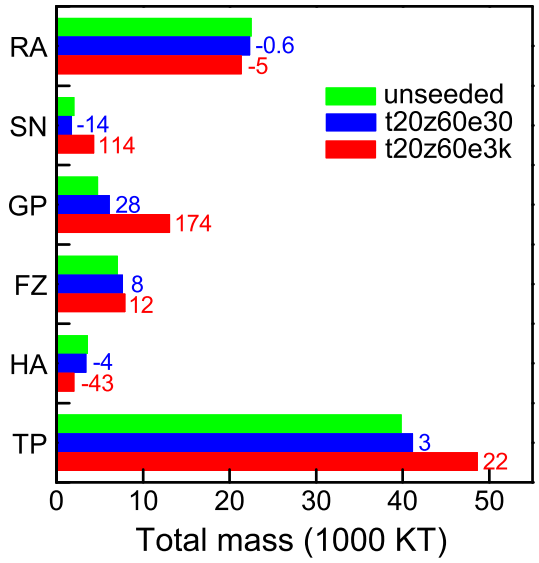

Figure 10. Accumulative total mass of the hydrometeor for the unseeded (green) and the seeded cases of t20z60e30 (blue) and t20z60e3k (red). RA, SN, GP, FZ, and HA represent the rain, snow, graupel, frozen drops, and hail, respectively. TP is the total precipitating hydrometeor. Numbers at the right side of columns are the percentage increase or decrease compared to the unseeded cases.

formation of less cloud ice at the later times. The question arises: can the high concentrations of graupel particles be transported upward to the stratosphere or not? This question is also important because sublimation/deposition of the injected graupel particles can provide an additional source/sink of water vapor. There are, in fact, many fewer graupel particles to enter the stratosphere crossing the tropopause in the seeded case than in the unseeded case since seeding reduced vertical transport, although more graupel was produced in the seeded case. Domain-averaged accumulative number concentrations of graupel particles for the stratosphere are found to be only 0.4 and 1.1 m^{-3} in t20z60e3k and the unseeded case, respectively. Those values are significantly lower as compared to the number concentration of ice crystals, which are 308.7 and 136.0 L^{-1} for the unseeded case and t20z60e3k, respectively. This indicates a negligible impact of seeding-induced change in upward transport of graupel particles through the tropopause on the water vapor content in the LS.

Compared to the unseeded case, the seeded case has more precipitation mass. Accumulated total mass of precipitating hydrometeors (the total of rain, snow, graupel, frozen drops, and hail) is 41,153 KT for t20z60e30 and 48,639 KT for t20z60e3k; both values are greater than the 39,824 KT for the unseeded case. The total precipitation mass is increased by 3% and 22%, respectively. In a shearing ambient wind field, the seeding-increased precipitation mass can enhance storm growth through enhanced downdrafts [*Simpson*, 1980]. This case, however, is characterized by weak wind shear in the low troposphere. Therefore, the loading effect of the increased precipitation mass in the seeded case suppresses the upward motion and causes the storm to have a weaker updraft as compared to the unseeded case. Despite the release of latent heat caused by AgI nucleation stimulates the storm updraft, this only occurs before 30 min, i.e., within 5 min after seeding. When the simulated storms have reached mature stages, the loading effect of precipitation mass dominates the storm vertical growth. Figure 10 shows clearly that graupel is the most main contributor for seeding-increased precipitation mass, accounting for 100% and 94% of the total increase in precipitation mass for t20z60e30 and t20z60e3k, respectively. This suggests that the seeding-increased graupel is mainly responsible for suppressed updrafts in seeded cases. Analysis mentioned above shows that graupel plays a key role in the context of seeding effects since it influences both microphysical cloud ice formation and vertical transport.

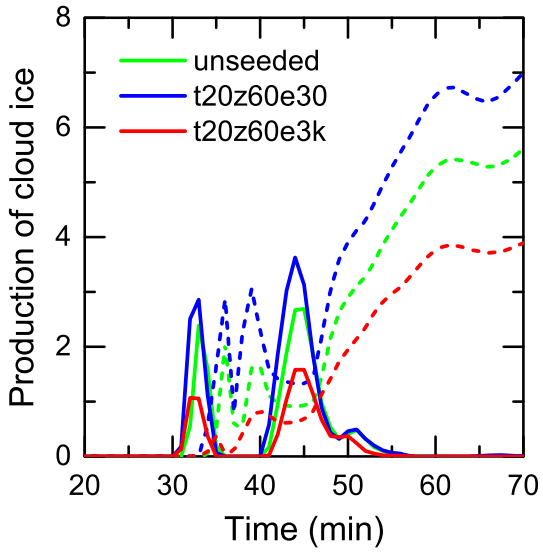

Figure 11. Domain-averaged production of cloud ice (unit in 10^{-8} g kg^{-1}) in the lower stratosphere due to deposition (solid line) and sublimation (dashed line) for the unseeded case (green) and the seeded cases of t20z60e30 (blue) and t20z60e3k (red). Sublimation dominates the ice microphysical processes in the LS, especially in the later stages of the simulations.

Results from the representative two experiments indicate that AgI seeding with a proper amount of

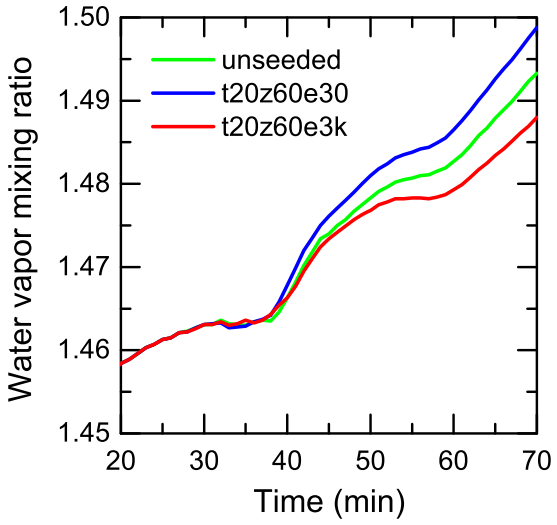

Figure 12. Time evolution of the domain-averaged water vapor mixing ratio (10^{-3} g kg^{-1}) in the lower stratosphere for the unseeded (green) and two seeded cases: t20z60e30 (blue) and t20z60e3k (red).

seeding agent could influence the cloud microphysics and dynamics of tropical overshooting deep convective storms and further cloud ice content entering the LS. The injected ice crystals can grow by deposition; however, sublimation dominates all cases, especially in the later stages (Figure 11). Compared with the unseeded case, sublimation is enhanced (reduced) in the light (heavy) seeding case due to increased (decreased) cloud ice concentrations; as a result, the water vapor content in the LS is increased (decreased) eventually (Figure 12). Note that the difference between unseeded and seeded cases in water vapor mixing ratio increases with time evolution. Considering that rather cloud ice is still left in the stratosphere at the end of simulation, thus, the stratospheric water vapor would be potentially altered further given more time.

5. Summary and Conclusions

This paper is an extension of previous work where we investigated the effects of atmospheric aerosols acting as CCN on stratospheric water vapor through overshooting deep convection. In the present work, we simulated the effects of artificial seeding with AgI on cloud microphysics and dynamics of overshooting deep convection. The primary goal is to examine whether the water vapor content in the lower stratosphere (LS) can be artificially modified by deliberate cloud seeding.

The results show that seeding done at the early stages of clouds has a significant effect on water vapor content in the LS and that either the water vapor may increase or decrease depending on seeding agent amount. It is found that the water vapor content is increased in light seeding case, whereas it is decreased in heavy seeding case, indicating that the response of the LS water vapor content to changes in the amount of seeding agent is nonlinear. Seeding done at the mature stage of clouds does not affect the LS water vapor content significantly.

Seeding affects on stratospheric water vapor with having dynamical and microphysical effects. In the absence of vertical wind shear, the seeding-enhanced loading effect of precipitation mass mainly in the form of graupel suppresses the upward motion and causes the storm to have weaker updrafts. The seeding-increased graupel particles enhance depletion of supercooled cloud water, and that reduces the formation of ice crystals later due to less homogenous freezing of droplets. The degree of reduction both in updrafts and cloud ice formation increases with the seeding agent amount. The combination of microphysical and dynamical effects caused by seeding makes more (less) upward transporting of ice crystals into the LS in the light (heavy) seeding scenarios, thereby resulting in the increase (decrease) in water vapor content of the stratosphere. The results also indicate that changes in graupel number and mass induced by seeding play a very important role in determining cloud properties and water vapor content in the stratosphere.

The present study focused on one overshooting event only. There is, in fact, a high occurrence frequency of the overshooting deep convection on a global scale, especially over land [*Iwasaki et al*., 2010]. Hence, seeding could potentially modify stratospheric water vapor to a greater extent if more overshooting convections are seeded.

It should be noted that the findings of this paper were limited to the AgI nucleation parameterizations proposed by *Hsie et al*. [1980]. Other nucleation parameterizations such as proposed by *Demott* [1995] and *Meyers et al*. [1995] should be examined in future studies due to the difference in nucleation modes. Moreover, the results of the present study were only based on a tropical thunderstorm under maritime climatic conditions. Modeling study by *Lin et al*. [2005] has shown significant differences in microphysical structures between thunderstorms in different climate regimes, such as the US High Plains vs maritime subtropics. Whether the conclusions in this paper can be extrapolated to other regions remains to be

confirmed, especially for midlatitude continental regions, in which overshooting deep convections also have an important role in regulating the water vapor content of the lower stratosphere [*Wang*, 2003; *Wang et al*., 2011]. We leave this subject for future work.

Acknowledgments

This work was primarily supported by the National Natural Science Foundation of China (41175118 and 40775005). Research results presented in this paper were jointly supported by the National Basic Research Program of China (2014CB441403 and 2013CB430105) and the China Special Fund for Meteorological Research in the Public Interest (GYHY201306040). Baojun Chen was also supported by the Jiangsu Collaborative Innovation Center for Climate Change. Simulations were performed on the IBM Blade cluster system in the High Performance Computing Center (HPCC) of Nanjing University. The authors acknowledge the SCOUT-O3/ACTIVE team for providing the sounding used in this research. They also thank Dr. Xiping Zeng and two anonymous reviewers for their critical yet constructive comments.

References

Chemel, C., M. R. Russo, J. A. Pyle, R. S. Sokhi, and C. Schiller (2009), Quantifying the imprint of a severe hector thunderstorm during ACTIVE/SCOUT-O3 onto the water content in the upper troposphere/lower stratosphere, *Mon. Weather Rev.*, *137*, 2493–2514, doi:10.1175/2008MWR2666.1.

Chen, B., and H. Xiao (2010), Silver iodide seeding impact on the microphysics and dynamics of convective clouds in the High Plains, *Atmos. Res.*, *96*, 186–207, doi:10.1016/j.atmosres.2009.04.001.

Chen, B., and Y. Yin (2011), Modeling the impact of aerosols on tropical overshooting thunderstorms and stratospheric water vapor, *J. Geophys. Res.*, *116*, D19203, doi:10.1029/2011JD015591.

Connolly, P. J., T. W. Choularton, M. W. Gallagher, K. N. Bower, M. J. Flynn, and J. A. Whiteway (2006), Cloud-resolving simulations of intense tropical Hector thunderstorms: Implications for aerosol–cloud interactions, *Q. J. R. Meteorol. Soc.*, *132*, 3079–3106, doi:10.1256/qj.05.86.

Cooper, W. A. (1986), Ice initiation in natural clouds, in *Precipitation Enhancement–A Scientific Challenge*, Meteor. Monogr., vol. 21, pp. 29–32, Am. Meteor. Soc., Boston, Mass.

Corti, T., et al. (2008), Unprecedented evidence for overshooting convection hydrating the tropical stratosphere, *Geophys. Res. Lett.*, *35*, L10810, doi:10.1029/2008GL033641.

Ćurić, M., D. Janc, and V. Vučković (2007), Cloud seeding impact on precipitation as revealed by cloud-resolving mesoscale model, *Meteorol. Atmos. Phys.*, *95*, 179–193, doi:10.1007/s00703-006-0202-y.

Ćurić, M., D. Janc, and V. Vučković (2008), Precipitation change from a cumulonimbus cloud downwind of a seeded target area, *J. Geophys. Res.*, *113*, D11215, doi:10.1029/2007JD009483.

DeMott, P. J. (1995), Quantitative descriptions of ice formation mechanisms of silver-iodide type aerosols, *Atmos. Res.*, *38*, 63–99.

de Reus, M., S. Borrmann, A. Bansemer, A. J. Heymsfield, R. Weigel, C. Schiller, V. Mitev, and W. Frey (2009), Evidence for ice particles in the tropical stratosphere from in-situ measurements, *Atmos. Chem. Phys.*, *9*, 6775–6792, doi:10.5194/acp-9-6775-2009.

Dessler, A. E., M. R. Schoeberl, T. Wang, S. M. Davis, and K. H. Rosenlof (2013), Stratospheric water vapor feedback, *Proc. Natl. Acad. Sci. U. S. A.*, *110*, 18,087–18,091, doi:10.1073/pnas.1310344110.

Ekman, A., A. Engström, and C. Wang (2007), The effect of aerosol composition and concentration on the development and anvil properties of a continental deep convective cloud, *Q. J. R. Meteorol. Soc.*, *133B*(627), 1439–1452, doi:10.1002/qj.108.

Fan, J., T. Yuan, J. M. Comstock, S. Ghan, A. Khain, L. R. Leung, Z. Li, V. J. Martins, and M. Ovchinnikov (2009), Dominant role by vertical wind shear in regulating aerosol effects on deep convective clouds, *J. Geophys. Res.*, *114*, D22206, doi:10.1029/2009JD012352.

Fan, J., J. M. Comstock, and M. Ovchinnikov (2010), The cloud condensation nuclei and ice nuclei effects on tropical anvil characteristics and water vapor of the tropical tropopause layer, *Environ. Res. Lett.*, *5*, 044005, doi:10.1088/1748-9326/5/4/044005.

Farley, R. D., H. Chen, H. D. Orville, and M. R. Hjelmfelt (2004), Numerical simulation of hail formation in the 28 June 1989 Bismarck thunderstorm. Part II: Cloud seeding results, *Atmos. Res.*, *71*, 81–113, doi:10.1016/j.atmosres.2004.03.006.

Grosvenor, D. (2010), Interactive comment on "Water vapour budget associated to overshoots in the tropical stratosphere: Mesoscale modelling study of 4–5 August 2006 during SCOUT–AMMA" by X. M. Liu et al, *Atmos. Chem. Phys. Discuss.*, *10*, C1348–C1351.

Grosvenor, D. P., T. W. Choularton, H. Coe, and G. Held (2007), A study of the effect of overshooting deep convection on the water content of the TTL and lower stratosphere from Cloud Resolving Model simulations, *Atmos. Chem. Phys.*, *7*, 4977–5002, doi:10.5194/acp-7-4977-2007.

Hong, Y., and P. Fan (1999), Numerical simulation study of hail cloud, Part I: The numerical model, *Acta Meteorol. Sin.*, *13*, 188–199.

Hsie, E.-Y., R. D. Farley, and H. D. Orville (1980), Numerical simulation of ice-phase convective cloud seeding, *J. Appl. Meteorol.*, *19*, 950–977.

Hu, Z., and G. He (1988), Numerical simulation of microphysical processes in cumulonimbus, Part I: Microphysical model, *Acta Meteorol. Sin.*, *2*, 471–489.

Iwasaki, S., T. Shibata, J. Nakamoto, H. Okamoto, H. Ishimoto, and H. Kubota (2010), Characteristics of deep convection measured by using the A-Train constellation, *J. Geophys. Res.*, *115*, D06207, doi:10.1029/2009JD013000.

Iwasaki, S., T. Shibata, H. Okamoto, H. Ishimoto, and H. Kubota (2012), Mixtures of stratospheric and overshooting air measured using A-Train sensors, *J. Geophys. Res.*, *117*, D12207, doi:10.1029/2011JD017402.

Klemp, J. B., and R. B. Wilhelmson (1978), The simulation of three-dimensional convective storm dynamics, *J. Atmos. Sci.*, *35*, 1070–1096, doi:10.1175/1520-0469(1978)035<1070:TSOTDC>2.0.CO;2.

Kong, F. Y., M. Y. Huang, and H. Y. Xu (1990), Three-dimensional numerical simulation of ice phase microphysics in cumulus clouds. Part I: Model establishment and ice phase parameterization (*in Chinese*), *Chin. J. Atmos. Sci.*, *14*, 441–453.

Kovačević, N., and M. Ćurić (2013), The impact of the hailstone embryos on simulated surface precipitation, *Atmos. Res.*, *132–133*, 154–163, doi:10.1016/j.atmosres.2013.05.013.

Levin, Z., and W. R. Cotton (Eds.) (2009), *Aerosol Pollution Impact on Precipitation: A Scientific Review*, 386 pp., Springer, New York, doi:10.1007/978-1-4020-8690-8.

Li, G., Y. Wang, and R. Zhang (2008), Implementation of a two-moment bulk microphysics scheme to the WRF model to investigate aerosol-cloud interaction, *J. Geophys. Res.*, *113*, D15211, doi:10.1029/2007JD009361.

Lin, Y. L., R. D. Farley, and H. D. Orville (1983), Bulk parameterization of the snow field in a cloud model, *J. Clim. Appl. Meteorol.*, *22*, 1065–1092, doi:10.1175/1520-0450(1983)022<1065:BPOTSF>2.0.CO;2.

Lin, H., P. K. Wang, and R. E. Schlesinger (2005), Three-dimensional nonhydrostatic simulations of summer thunderstorms in the humid subtropics versus High Plains, *Atmos. Res.*, *78*, 103–145, doi:10.1016/j.atmosres.2005.03.005.

Liu, X. M., E. D. Rivière, V. Marécal, G. Durry, A. Hamdouni, J. Arteta, and S. Khaykin (2010), Stratospheric water vapour budget and convection overshooting the tropopause: Modelling study from SCOUT-AMMA, *Atmos. Chem. Phys.*, *10*, 8267–8286, doi:10.5194/acp-10-8267-2010.

Meyers, P. M., P. J. DeMott, and W. R. Cotton (1995), A comparison of seeded and nonseeded orographic cloud simulations with an explicit cloud model, *J. Appl. Meteorol.*, *34*, 834–846.

Morrison, H., J. A. Curry, and V. I. Khvorostyanov (2005), A new double-moment microphysics parameterization for application in cloud and climate models, Part I: Description, *J. Atmos. Sci.*, *62*, 1665–1677, doi:10.1175/JAS3446.1.

NRC (National Research Council) (2003), *Critical Issues in Weather Modification Research*, National Academies Press, Washington, D. C.

Orville, H. D., and J. M. Chen (1982), Effects of cloud seeding, latent heat of fusion, and condensate loading on cloud dynamics and precipitation evolution: A numerical study, *J. Atmos. Sci.*, *39*, 2807–2827.
Qiu, J., and D. Cressey (2008), Taming the sky, *Nature*, *453*, 970–974.
Ravishankara, A. R. (2012), Water vapor in the lower stratosphere, *Science*, *337*, 809–810, doi:10.1126/science.1227004.
Rogers, R. R., and M. K. Yau (1989), *A Short Course in Cloud Physics*, 3rd ed., pp. 293, Pergamon Press, Oxford.
Rosenfeld, D., and W. L. Woodley (1993), Effects of cloud seeding in West Texas: Additional results and new insights, *J. Appl. Meteorol.*, *32*, 1848–1866.
Simpson, J. (1980), Downdrafts as linkages in dynamic cumulus seeding effects, *J. Appl. Meteorol.*, *19*, 477–487.
Solomon, S., K. H. Rosenlof, R. W. Portmann, J. S. Daniel, S. M. Davis, T. J. Sanford, and G.-K. Plattner (2010), Contributions of stratospheric water vapor to decadal changes in the rate of global warming, *Science*, *327*, 1219–1223, doi:10.1126/science.1182488.
Tao, W.-K., J.-P. Chen, Z. Li, C. Wang, and C. Zhang (2012), Impact of aerosols on convective clouds and precipitation, *Rev. Geophys.*, *50*, RG2001, doi:10.1029/2011RG000369.
Thompson, G., P. R. Field, R. M. Rasmussen, and W. D. Hall (2008), Explicit forecasts of winter precipitation using an improved bulk microphysics scheme. Part II: Implementation of a new snow parameterization, *Mon. Weather Rev.*, *136*, 5095–5115, doi:10.1175/2008MWR2387.1.
Wang, P. K. (2003), Moisture plumes above thunderstorm anvils and their contributions to cross tropopause transport of water vapor in midlatitudes, *J. Geophys. Res.*, *108*(D6), 4194, doi:10.1029/2002JD002581.
Wang, P. K., S. H. Su, Z. Charvát, J. Šťástka, and H. M. Lin (2011), Cross tropopause transport of water by mid-latitude deep convective storms: A review, *Terr. Atmos. Ocean. Sci.*, *22*, 447–462, doi:10.3319/TAO.2011.06.13.01(A).
Xue, L., A. Hashimoto, M. Murakami, R. Rasmussen, S. A. Tessendorf, D. Breed, S. Parkinson, P. Holbrook, and D. Blestrud (2013), Implementation of a silver iodide cloud-seeding parameterization in WRF. Part I: Model description and idealized 2D sensitivity tests, *J. Appl. Meteorol. Climatol.*, *52*, 1433–1457, doi:10.1175/JAMC-D-12-0148.1.
Zeng, X., W.-K. Tao, S. W. Powell, R. A. Houze Jr., P. Ciesielski, N. Guy, H. Pierce, and T. Matsui (2013), A comparison of the water budgets between clouds from AMMA and TWP-ICE, *J. Atmos. Sci.*, *70*, 487–503, doi:10.1175/JAS-D-12-050.